Journal of Molecular and Cellular Cardiology 205 (2025) 13–23

Contents lists available at ScienceDirect

Journal of Molecular and Cellular Cardiology

journal homepage: www.elsevier.com/locate/yjmcc

# The BAG3-HSP70-CHIP axis controls the degradation of TGFBR2 in cardiac fibroblasts

Margaretha A.J. Morsink [a], Josephine M. Watkins [a], Katelyn Zhu [a], Xiaokan Zhang [b], Lori J. Luo [a], Barry M. Fine [b], Bryan Z. Wang [a,b,*], Gordana Vunjak-Novakovic [a,b,c,**]

[a] Department of Biomedical Engineering, Columbia University, New York, NY, USA
[b] Department of Medicine, Columbia University, New York, NY, USA
[c] College of Dental Medicine, Columbia University, New York, NY, USA

ARTICLE INFO

*Keywords:*
Fibrosis
TGF-β signaling
BAG3
Cardiac fibroblast
HSP70
E3 ligase

ABSTRACT

Transforming Growth Factor Beta (TGF-β) is a master regulator of cardiac fibrosis, in part through the type II TGF-β receptor (TGFBR2) which initiates signaling after ligand binding. We previously identified the co-chaperone protein Bcl2-associated athanogene (BAG3) as a modulator of TGFBR2 through ubiquitination and proteasomal degradation. However, the E3 ligase of TGFBR2 was not known. Using induced pluripotent stem cell-derived cardiac fibroblasts, we identified C-terminal interacting protein of HSP70 (CHIP) as an E3 ubiquitin ligase utilized by BAG3 for TGFBR2 degradation in cardiac fibroblasts. Overexpression of CHIP significantly decreased TGFBR2 stability, while inhibition of CHIP led to increased sensitivity to TGF-β and subsequent promotion of a fibrogenic program. Further, the BAG3-HSP70 interaction was crucial to this process, as disruption of the axis increased TGFBR2 stability and sensitivity to TGF-β signaling. Together, these findings demonstrate that the BAG3-HSP70-CHIP axis controls TGF-β signaling in cardiac fibroblasts and could serve as a new therapeutic target for cardiac fibrosis.

## 1. Introduction

Pathological fibrosis, the process of excessive extracellular matrix deposition, is a histological hallmark of end-stage cardiovascular diseases, from ischemic heart disease to genetic cardiomyopathies [1,2]. Damaged cardiomyocytes are replaced by fibrotic scar, which leads to reduced tissue compliance, decreased mechanical function, and accelerates the progression to heart failure [1]. The Transforming Growth Factor β (TGF-β) pathway is a well-studied master regulator of fibrosis [3,4]. TGF-β is involved in many cellular processes, including proliferation, apoptosis, cell growth, and homeostasis [4,5]. The initiator of all signaling within this pathway is the transmembrane type II TGF-β receptor (TGFBR2). Interactions of TGF-β ligand and TGFBR2 result in dimerization with the TGFBR1 co-receptor and downstream substrate phosphorylation events, including SMAD2 and SMAD3, which upregulate transcription of several pro-fibrotic genes, including collagen 1 (COL1A1) [6].

Control of the TGF-β pathway is tightly regulated by various mechanisms, such as protein degradation, which is facilitated by the ubiquitin system. Ubiquitination occurs through the cascade of three separate enzymes: the E1 ubiquitin-activating enzyme, the E2 ubiquitin-conjugating enzyme, and the E3 ubiquitin ligase. Within this system, the specificity and complexity of ubiquitination is derived from the E3 ligase, which selects the substrate for ubiquitination [7]. The number of each enzyme type demonstrates this clearly: in humans, there are only two known E1 enzymes, approximately 40 E2 enzymes, and over 600 E3 ligases that have been identified. Within the TGF-β signaling pathway, researchers have identified E3 ligase WWP2 as a mediator of degradation of SMAD2 [8], and the C-terminal interacting protein of HSP70 (CHIP) as a mediator for the degradation of SMAD3 [9]. Additionally, SMAD ubiquitin regulatory factor 1 (SMURF1) and SMURF2 are E3 ligases for SMAD1 and SMAD5 [10].

Bcl2-associated athanogene 3 (BAG3) is a regulator of cardiac proteostasis. BAG3 is a co-chaperone protein that forms a complex with client proteins and heat shock protein 70 (HSP70) [11]. Loss-of-function variants of BAG3 give rise to cardiomyopathies [12–14]. Moreover,

* Corresponding author at: Department of Medicine, Columbia University, New York, NY, USA.
** Corresponding author at: Department of Biomedical Engineering, 622 West 168th Street VC12-234, 10032, USA.
*E-mail addresses:* bzw2101@cumc.columbia.edu (B.Z. Wang), gv2131@columbia.edu (G. Vunjak-Novakovic).

https://doi.org/10.1016/j.yjmcc.2025.06.003
Received 9 December 2024; Received in revised form 7 April 2025; Accepted 4 June 2025
Available online 5 June 2025

BAG3 levels are diminished in patients with non-genetic heart failure [15–17]. In cardiomyocytes, BAG3 is responsible for the turnover of several sarcomere proteins at the *Z*-disk, including Filamin-C [16,18,19]. In recent work, we identified BAG3 as a regulator of TGFBR2 degradation through the proteasomal pathway within cardiac fibroblasts. Loss of BAG3, therefore, increased TGFBR2 levels and subsequent TGF-β signaling and fibrosis [17].

However, BAG3 lacks intrinsic E3 ligase activity. Rather, it recruits E3 ligases for protein disposal. The E3 ligase through which BAG3 regulates TGFBR2 is not known. In this study, we utilized our established model of BAG3 in iPSC-derived cardiac fibroblasts to identify CHIP as an E3 ligase that BAG3 recruits to modulate TGFBR2 degradation. We also found that the BAG3-HSP70 axis is critical to this process. Together, we show that disruption of the BAG3-HSP70-CHIP axis leads to the progression of cardiac fibrosis.

## 2. Methods

### 2.1. 2.1 iPSC culture

Human induced pluripotent stem cells (iPSC) were maintained in mTeSR Plus medium (Stem Cell Technologies) with 1 % penicillin/streptomycin (Gibco) on Matrigel-coated plates and passaged every 3–4 days using 0.5 mM EDTA and treated with 5 μM Rock inhibitor (RI) for one day after passaging. The male isogenic wild-type and BAG3 knockout ($BAG3^{-/-}$) WTC [20] lines of iPS cells were obtained from Dr. Bruce Conklin by MTA between Columbia University and the Gladstone Institute.

### 2.2. Cardiac fibroblast differentiation and culture

The wild-type and BAG3 KO iPSCs were differentiated into cardiac fibroblasts (iCFs) using an established protocol [21]. Briefly, iPSCs were replated at a density of 1.5E06 cells per well in a 6-well plate in mTeSR Plus with RI and refreshed to mTeSR Plus the following day. Two days after the initial replate, the cardiac progenitor cell differentiation was initiated by switching to chemically defined medium with 3 components (CDM3) [22]. The cells were subjected to 4–8 μM CHIR9902 (Tocris) for 1 day, CDM3 for 1 day, and CDM3 with 2 μM Wnt-C59 (Tocris) for 2 days. On day 5, the cells were dissociated using Accutase (Stem Cell Technologies) and replated at 20,000 cells/$cm^2$ on Matrigel-coated 6 well plates in Advanced DMEM with 2 μM retinoic acid, 5 μM CHIR, and 5 μM RI. On Day 6, the medium was refreshed to Advanced DMEM +5 μM CHIR and 2 μM retinoic acid for two days. On Day 8, cells were transferred to Advanced DMEM, and then cultured from Day 11 to Day 14 in Advanced DMEM with 2 μM SB431542 (Tocris). On Day 14, cells were split at a density of 10,000/$cm^2$ into a Fibroblast Growth Medium 3 (Promocell) supplemented with 20 ng/mL FGF2 (Peprotech) and 10 μM SB431542 until Day 20. Differentiated cardiac fibroblasts were maintained in Fibroblast Growth Medium 3 (FGM3) and cultured up to passage 4.

### 2.3. Transfection of siRNA and plasmids

Transfections were performed on iCFs that were approximately 50–70 % confluent. siRNA of CHIP (Thermofisher, ID: 195025) and WWP2 (Thermofisher, ID: 200486) were transfected using Lipofectamine RNAiMAX following manufacturer's protocol. DNA constructs of FLAG-tagged full-length BAG3 and BAG3 lacking the functional domains, as well as the V5-tagged TGFBR2, and MYC-tagged CHIP and WWP2 used in this study were purchased from and cloned by Vectorbuilder (www.vectorbuilder.com). V5-PRKAR1A was previously published [23]. DNA plasmids were transfected using Viafect (Promega) following manufacturer's protocol with a ratio of 6:1 transfection reagent to plasmid (*v/w*).

### 2.4. Luciferase assay

Cells were transfected with SBE4-Luc (Addgene #16495) and pRL (Promega E2261) at a 1:1 ratio using Viafect as described. 24 h after transfection, media was refreshed with or without 10 ng/mL TGFβ1 (Peprotech 100-21C). 24 h later, luciferase activity was analyzed using the Dual-Glo Luciferase Assay Kit (Promega E2920) according to the manufacturer's instructions, using the Synergy H1 Plate Reader (BioTek).

### 2.5. Treatments of iCFs

iCFs were treated with 10 ng/mL TGF-β1 (Peprotech) for 15 min up to 48 h. The cells were subjected to 1 μM JG-98 (Selleck Chemicals) or the equivalent volume of DMSO for 48 h.

### 2.6. Western blot

Protein samples were obtained by adding Pierce IP Lysis Buffer (Thermofisher #87787) containing protease and phosphatase inhibitors (Thermofisher #78442) on iCFs and scraped into the plate. The collected lysate was intermittently vortexed for 20 min while remaining on ice. Cell debris was removed by centrifugation of the lysate at 16,000*g* for 10 min.

The protein content in the supernatant was quantified using the Pierce BCA kit (Thermofisher). Lysates were mixed with 4× Laemmli buffer and boiled at 95 °C for 5 min and 15 μg total protein was loaded in a 4–20 % Tris-glycine gel (Thermofisher, XP04205BOX). The gels were transferred onto 0.2 μm nitrocellulose membranes and blocked in 5 % non-fat dry milk. Incubation with primary antibodies was done overnight at 4 °C in 5 % BSA in TBS with 0.1 % Tween 20 (TBST).

The following primary antibodies were used: phospho-SMAD2 (Cell Signaling Technologies, #3108, 1:1000), total SMAD2/SMAD3 (Cell Signaling Technologies, #3102, 1:1000), phospho-SMAD3 (Cell Signaling Technologies, #9520, 1:500), phospho-p38 (Cell Signaling Technologies, #4511, 1:1000), total p38 (Cell Signaling Technologies, #8690, 1:1000), V5 (Cell Signaling Technologies, #13202. 1:1000), MYC (Cell Signaling Technologies, #2272, 1:1000), WWP2 (Proteintech, #12197–1-AP, 1:1000), HSPB8 (Proteintech, #15287–1-AP, 1:1000), BAG3 (Proteintech, #10599–1-AP, 1:3000), HSP70 (Proteintech, #10995–1-AP, 1:2000), TGFBR2 antibody (Thermo Fisher Scientific, 701,683, 1:250 in TBST), and CHIP (Santa Cruz, #sc-133,083, 1:100), HRP-conjugated β-actin (Cell Signaling Technologies, #5125, 1:1000), and HRP-conjugated GAPDH (Cell Signaling Technologies, #3683, 1:1000).

The next day, the membranes were washed and blotted with an HRP-linked mouse or rabbit secondary antibody (1:5000) in milk for 1 h at room temperature. Western blot membranes were imaged on a Licor Odyssey Fc system, after incubation with ECL, and band intensity was quantified in the ImageStudio Lite Software (v5.2). For blots involving the detection of endogenous TGFBR2, whole-cell lysates were prepared following the protocol detailed in our previous study [17]. Briefly, cells were lysed in 1 % sodium dodecyl sulfate in 10 mM Tris-HCl buffer containing 1 mM sodium orthovanadate boiled for 20 min, and homogenized by passing through a 26.5-gauge needle 10 times. After centrifugation at 16,000*g* for 10 min, the supernatant protein concentration was measured with BCA, to obtain 40 μg per lane and mixed with 4× Laemmli buffer.

### 2.7. Immunoprecipitation

For all immunoprecipitation studies, samples were lysed in a custom buffer (MS lysis buffer) containing 0.5 %(*v/v*) NP-40 detergent, 150 mM sodium chloride, 10 mM potassium chloride, 1.5 mM magnesium chloride, and 10 mM Tris-HCl buffer supplemented with protease and phosphatase inhibitors. Lysate was placed on ice for 20 min with

intermittent vortexing, and centrifuged at 16,000*g* for 10 min at 4 °C. The supernatant was removed to a clean tube and protein concentration quantified with Pierce BCA Kit (ThermoFisher). Each immunoprecipitation reaction contained 300-500 μg of equivalent protein.

FLAG (Sigma M8823) and MYC (Pierce #88842) conjugated magnetic beads were used for immunoprecipitation, according to the manufacturer's protocol. Briefly, 20 μL of beads were used per reaction and incubated with samples overnight at 4 °C. The next day, beads were washed with MS lysis buffer 10 times, eluted in 0.1 M glycine-HCl pH 2.8 for 25 min with agitation, and quenched in 1 M Tris-HCl. Samples were reduced in 4× Laemmli and boiled for 5 min at 95 °C for subsequent Western Blot.

### 2.8. Chase studies

Control samples were washed in PBS and subsequently lysed on the plate in 2× Laemmli buffer and boiled for 20 mins at 95 °C. iCFs were subsequently treated with 50 μg/mL cycloheximide (Sigma C4859) in FGM3 and lysed similarly at timepoints 1 h, 3 h, and 6 h. The samples were boiled for 20 min at 95 °C and stored at −20 °C or directly used for Western Blot.

### 2.9. Immunofluorescence

Cells were fixed by 4 % formaldehyde (Sigma, Cat no. 252549) in PBS for 15 mins at room temperature and subsequently washed three times for 5 mins with PBS. Afterwards, samples were permeabilized in 0.25 % (*v*/v) Triton X-100 (Sigma-Aldrich, Cat no. T8787-250ML) for 10 mins at room temperature and blocked using the blocking buffer consisting of 10 % (v/v) FBS in PBS for 1 h at room temperature under gentle shaking. The primary antibodies were diluted in 5 % BSA in PBS and incubated overnight at 4 °C. The primary antibodies used were anti-Rabbit Collagen I (1:1000, Abcam, ab34710), anti-Mouse ASMA (1:500, Abcam, ab7817), anti-chicken Vimentin (1:1000, Abcam, ab24525), anti-Mouse Ki67 (1:1000, Cell Signaling Technologies, #9449S). The next day, samples were washed three times for 5 mins in DPBS. The secondary antibodies (Goat anti-Mouse IgG Alexa Fluor 594, Invitrogen; Goat anti-Rabbit IgG Alexa Fluor 647, Invitrogen, Goat anti-Chicken IgG Alexa Fluor 388, Invitrogen) were diluted 1:2000 in 5 % BSA in PBS and incubated for 60 min at room temperature in the dark under gentle shaking. Subsequently, three washes of 5 mins in DPBS were performed. The samples were counterstained using DAPI (1:1000 in DPBS, BD Pharmingen). Samples were imaged using the Nikon A1 Confocal Microscope. The percentage of proliferative cells was determined by the number of Ki67-positive nuclei compared to DAPI-stained nuclei, as analyzed by CellProfiler [24].

### 2.10. RT-qPCR

mRNA was isolated from treated cells in a 12 wells plate using the RNeasy Mini Kit (Qiagen, Cat no. 74106) according to the manufacturer's instruction. RNA quality was ensured with proper 260/230 ratio between 1.8 and 2.2 using the NanoDrop One (Thermofisher). cDNA samples were obtained from 1 μg RNA using High Capacity cDNA Reverse Transcription Kit (Applied Biosystems, Cat no. 4368813) according to the manufacturer's instructions. Reverse transcriptase quantitative polymerase chain reaction (RT-qPCR) was performed with 5 ng cDNA per sample, 10 μM of forward and reverse primer (see Table 1), and Fast SYBR Green Master Mix (Applied Biosystems, Cat no. 4385612) in a 96 wells plate (Applied Biosystems, Cat no. 4346906). Thermal cycling was performed in a StepOne Plus Real Time PCR System (Applied Biosystems) using 40 cycles of two-step PCR protocol of 95 °C melting for 3 s and 60 °C annealing and extension for 30 s, prior to an initial hot start at 95 °C for 20 s.

**Table 1**
Primer sets for RT-qPCR.

| Gene of Interest | Oligo Sequence (5′ ➔ 3′) |
|---|---|
| β-ACTIN Fw | CACCATTGGCAATGAGCGGTTC |
| β-ACTIN Rev | AGGTCTTTGCGGATGTCCACGT |
| ACTA2 Fw | CCGACCGAATGCAGAAGGA |
| ACTA2 Rev | ACAGAGTATTTGCGCTCCGAA |
| COL1A1 Fw | GATTCCCTGGACC TAAAGGTGC |
| COL1A1 Rev | AGCCTCTCCATCT TTGCCAGCA |
| CHIP Fw | AGGCCAAGCACGACAAGTACAT |
| CHIP Rev | CTGATCTTGCCACACAGGTAGT |
| FN-EDA Fw | TCCAAGCGGAGAGAGT |
| FN-EDA Rev | GTGGGTGTGACCTGAG |
| IL-11 Fw | GGACCACAACCTGGATTCCCTG |
| IL-11 Rev | AGTAGGTCCGCTCGCAGCCTT |
| LOX Fw | GATACGGCACTGGCTACTTCCA |
| LOX Rev | GCCAGACAGTTTTCCTCCGCC |
| TIMP1 Fw | GAGAGACACCAGAGAACCCAC |
| TIMP1 Rev | CCACAGCAACAACAGGATGC |
| TIMP3 Fw | ACCGAGGCTTCACCAAGATG |
| TIMP3 Rev | CATCATAGACGCGACCTGTCA |

### 2.11. Total collagen secretion assay

Supernatants of iCFs cultured on soft 8 kPa plates were collected, and collagen was concentrated using a concentrating solution (Chondrex #90626) according to the manufacturer's instructions. Secreted collagen was measured using Sirius Red Total Collagen Detection Kit (Chondrex #9062) from the absorbance at 530 nm, using the Synergy H1 Plate Reader (BioTek).

### 2.12. Collagen ELISA

Collagen I α1 concentration was determined using ELISA (Abcam, ab210966), according to manufacturer's protocol. Briefly, the supernatant of iCFs cultured on soft 8 kPa plates treated with DMSO or JG-98, respectively, was diluted 1:1000 in sample diluent. Absorbance was measured at 450 nm using the Synergy H1 Plate Reader (BioTek). The collagen I α1 concentration was subsequently normalized to the cell density as determined by BCA assay (Pierce).

### 2.13. Analysis of global mass spec data

Detailed methods of BAG3 interactome assessment and generation of the dataset is available in our prior study [17]. Briefly, wild-type BAG3 containing a 3× FLAG tag and an empty vector were overexpressed in *BAG3*$^{-/-}$ iCFs. BAG3 was immunoprecipitated using FLAG beads and the eluate was sent for mass spectrometry analysis. Significantly changed protein abundances were determined by *t*-test analysis (FDR < 0.01) to identify proteins demonstrating statistically significant changes in abundance.

### 2.14. Statistical analysis

Statistical significance was evaluated by a Student's t-test, one-way ANOVA followed by Bonferroni's post-hoc test, or a two-way ANOVA followed by Sidak's post-hoc test after confirming normal distribution by the Shapiro-Wilk test with $\alpha = 0.05$, using GraphPad Prism 10.4.0 (GraphPad Software, La Jolla, CA). For non-Gaussian distributed samples, we performed the Kruskal-Wallis test followed by Dunn's test to test for statistical differences. The *p*-value of less than 0.05 was considered statistically significant. *P*-values are displayed in the graphs. Error bars indicate standard deviation. Specific statistical analysis per graph is indicated in the figure captions.

## 3. Results

### 3.1. CHIP is identified as E3 ubiquitin ligase of TGFBR2

Given that direct ligase-substrate binding is required for ubiquitination, we hypothesized that the specific E3 ligase of TGFBR2 functions in close proximity to BAG3. We explored our existing interactome data of FLAG-tagged BAG3 overexpressed in *BAG3*$^{-/-}$ cardiac fibroblasts derived from induced pluripotent stem cells (iCFs) [17]. We identified five candidate E3 ligases: CHIP/STUB1 (referred to as CHIP),

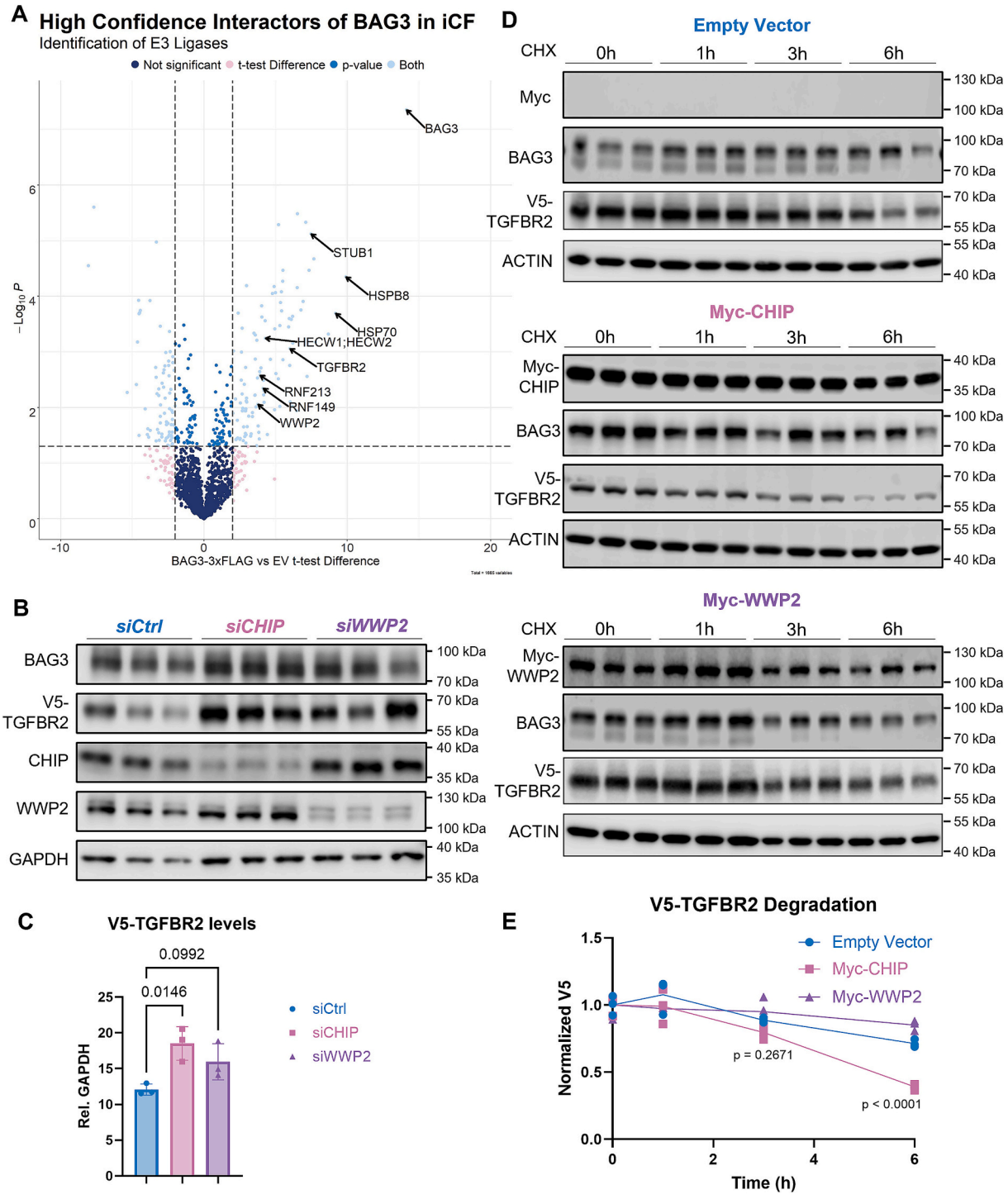


**Fig. 1.** CHIP is identified as an E3 ligase of TGFBR2 in iCFs. A) Proteomic analysis of BAG3 immunoprecipitation identified the high-confidence interactors with BAG3 in iCFs, including several E3 ligases. B) Silencing of CHIP and WWP2 and their effects on V5-TGFBR2 levels on Western Blot. C) Densitometry quantification of V5-TGFBR2 levels upon silencing of CHIP or WWP2. Significance indicated by one-way ANOVA with post-hoc Dunnett's. Error bars represent the mean with standard deviation. D) Cycloheximide chase studies over the course of 6 h of V5-TGFBR2 upon overexpression of an Empty Vector, MYC-CHIP, or MYC-WWP2 construct on Western Blot. E) Densitometry quantification of V5-TGFBR2 degradation rate from (D), normalized to 0 h per condition. Significance indicated by two-way ANOVA with post-hoc Šídák. *p*-values less than 0.05 are considered statistically significant. In all experiments, $n = 3$ biological triplicates, where n indicates a single well of cells.

HECW1/2, RNF149, RNF213, and WWP2 (Fig. 1A). Based on previous reports, CHIP and WWP2 were the likely candidates for the E3 ligase and we selected these for further study [8,25,26].

To identify the turnover and levels of TGFBR2, we overexpressed V5-tagged TGFBR2 in wild-type iCFs. We confirmed that the V5-TGFBR2 was functional in the TGF-β signaling pathway, as evidenced by the increased activity of an SBE4 luciferase reporter (Supplementary Fig. 1A). To study the candidate E3 ligases of TGFBR2, we co-transfected V5-TGFBR2 and siRNAs targeted to WWP2 and CHIP (Supplementary Fig. 1B, C). Interestingly, silencing CHIP resulted in significant upregulation of V5-TGFBR2 protein expression, whereas silencing WWP2 did not increase V5-TGFBR2 levels significantly (Fig. 1B, C). To exclude the possibility of the lysine residue in the V5 tag as a possible site for ubiquitination that would interfere with the assay, we further co-transfected siRNAs with a V5-tagged unrelated gene (*PRKAR1A*) plasmid and demonstrated that the expression of this construct did not change upon silencing of CHIP and WWP2 (Supplementary Fig. 1D).

We next examined the effects of CHIP and WWP2 overexpression on the stability of TGFBR2. By inhibiting protein translation with cycloheximide (CHX), we assayed the stability and degradation of V5-TGFBR2 levels over time. Overexpression of CHIP significantly accelerated the degradation rate of TGFBR2, while overexpression of WWP2 did not have an effect compared to the empty vector control (Fig. 1D, E). Together these knockdown and overexpression studies suggested CHIP as a regulator of TGFBR2 degradation.

To further validate CHIP as an E3 ligase for TGFBR2, we examined TGFBR2 ubiquitination upon silencing of CHIP. Immunoprecipitation of V5-TGFBR2 after co-transfection with siCHIP indeed demonstrated significantly decreased ubiquitination (Fig. 2A,B). V5-TGFBR2 levels were again upregulated upon silencing of CHIP (Fig. 2C). Notably, we confirmed the presence of a CHIP-TGFBR2-BAG3-HSP70 interaction through immunoprecipitation of Myc-CHIP (Fig. 2D). Conversely, Myc-WWP2 did not interact with V5-TGFBR2 (Supplementary Fig. 2). We further confirmed the upregulation of endogenous TGFBR2 levels upon silencing of CHIP (Fig. 2E,F). Taken together, these data support that CHIP, rather than WWP2, is an E3 ligase of TGFBR2 in cardiac fibroblasts.

### 3.2. *BAG3 and its interaction with HSP70 are required for TGFBR2 degradation by CHIP*

CHIP is named after its interaction with HSP70 in a chaperone-dependent manner [27]. Thus, after the identification of CHIP as an E3 ligase of TGFBR2, we investigated the role of the BAG3-HSP70 complex in this process. We co-expressed V5-TGFBR2 and Myc-CHIP in *BAG3* knock-out iCFs and assessed TGFBR2 turnover. In contrast to wild-type iCFs, overexpression of CHIP did not significantly accelerate the turnover of V5-TGFBR2 in *BAG3*$^{-/-}$ iCFs (Fig. 3A,B), suggesting that BAG3 is required for the CHIP-mediated degradation of TGFBR2.

BAG3 is a multi-domain protein with several functional domains, including a BAG domain at the C-terminus, a WW domain, a proline-rich domain (PxxP), and two IPV domains that bind HSPB8. We further assessed the contributions of BAG3's functional domains (Supplementary Fig. 3A) to TGFBR2 degradation. To this end, we designed FLAG-tagged BAG3 plasmids containing deletions of the WW, IPV, PxxP, and BAG domains and confirmed disruption of the known binding interactions between HSP70 and HSPB8 (Supplementary Fig. 3B). Next, we overexpressed these plasmids in BAG3$^{-/-}$ iCFs to parse out the effects of the mutant-BAG3 plasmids and the full-length BAG3. Interestingly, overexpression of any BAG3 protein significantly decreased the protein expression of V5-TGFBR2, with the greatest decrease found for the wild-type BAG3 (Fig. 3C,D). Conversely, deletion of any of these functional domains within BAG3 attenuated the effect on V5-TGFBR2, particularly in the ΔBAG variant. This is in line with our previous

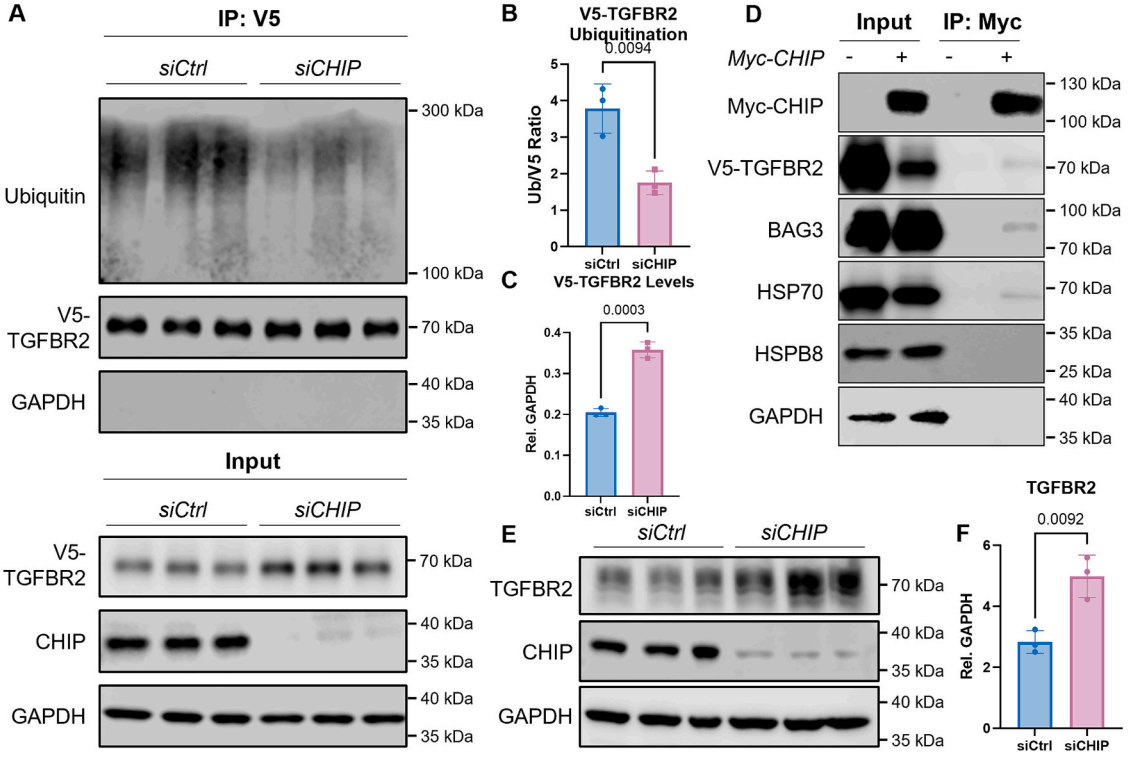


**Fig. 2.** Validation of CHIP as specific E3 ligase of TGFBR2 in iCFs. A) Silencing of CHIP reduces TGFBR2 ubiquitination. B) Quantification of ubiquitination using densitometry, normalized to immunoprecipitated V5. C) Quantification of V5-TGFBR2 within input samples of (A). D) Immunoprecipitation of Myc-CHIP identifies V5-TGFBR2 as an interactor while confirming the known interactors HSP70 and BAG3. E) Western blot of endogenous TGFBR2 upon silencing of CHIP, with densitometry quantification in F). Significance indicated by unpaired two-tailed Student's *t*-test. Error bars represent the mean with standard deviation. *p*-values less than 0.05 are considered statistically significant. For all quantitative experiments, $n = 3$, where n indicates a single well of cells, thus presenting biological triplicates.

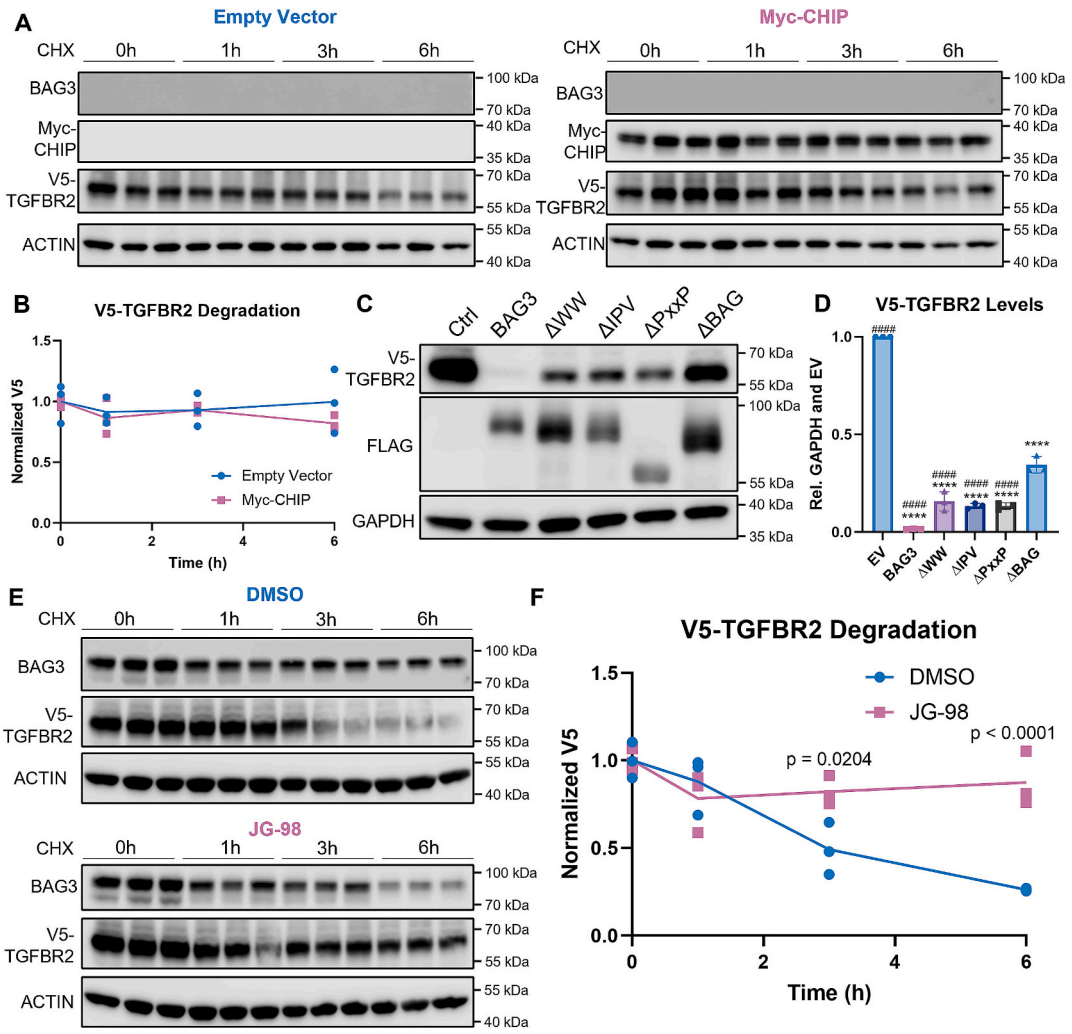


**Fig. 3.** BAG3 and its interaction with HSP70 are required for TGFBR2 degradation. A) Cycloheximide chase study of V5-TGFBR2 in BAG3 knock-out iCFs shows that despite overexpression of Myc-CHIP, BAG3 is still required for degradation. B) Densitometry of the degradation rate of V5-TGFBR2 from (A), normalized to 0 h per condition. Significance indicated by two-way ANOVA with post-hoc Šídák. C) Effect of mutant BAG3 plasmids on V5-TGFBR2 and in D) the quantified densitometry indicates remaining levels of V5-TGFBR2 upon addition of mutant BAG3 plasmids. **** indicates $p < 0.0001$ compared to EV, whereas #### indicates $p < 0.0001$ compared to ΔBAG by one-way ANOVA with post-hoc Dunnett's. E) JG-98 increases TGFBR2 stability in wild-type iCFs. F) Densitometry quantification of the degradation rate of V5-TGFBR2 from (E), normalized to 0 h per condition. Significance indicated by two-way ANOVA with post-hoc Šídák. Error bars represent the mean with standard deviation. *p*-values less than 0.05 are considered statistically significant. For all experiments, $n = 3$, where n indicates a single well of cells, thus presenting biological triplicates.

finding that the E455K mutation in the BAG domain (which disrupts HSP70 binding), reduces the ubiquitination of TGFBR2 when compared to wild-type BAG3 [17]. As further evidence, we chemically disrupted the BAG3-HSP70 interaction using the small molecule JG-98 in wild-type iCFs [28]. JG-98 significantly increased the stability of V5-TGFBR2 (Fig. 3E,F). Together, these data suggest that the BAG3-HSP70 axis is required for the turnover of TGFBR2 by CHIP.

### 3.3. *Inhibition of CHIP and the BAG3-HSP70 Axis increase sensitivity to TGFβ Signaling*

We next explored if modulating CHIP and the BAG3-HSP70 axis could significantly alter TGF-β signaling *via* TGFBR2 in wild-type iCFs. We examined the phosphorylation events downstream of TGF-β ligand binding to TGFBR2 in response to silencing of CHIP and inhibition of the BAG3-HSP70 axis by JG-98 (Fig. 4A,B). Silencing of CHIP and treatment with JG-98 significantly increased SMAD2, SMAD3, and p38 phosphorylation, consistent with our previous findings of BAG3 loss in iCFs (Fig. 4C-E, G-I). In addition, silencing of CHIP and exposure to JG-98 in wild-type iCFs both increased the responsiveness to TGF-β measured by a smad-binding element (SBE4) luciferase reporter (Fig. 4F,J). In sum, these data provide further evidence that the BAG3-HSP70-CHIP axis negatively regulates TGF-β signaling through TGFBR2 degradation.

### 3.4. *Inhibition of the BAG3-HSP70 Axis promotes a fibrogenic program in cardiac fibroblasts*

JG-98 has been investigated as an anti-neoplastic agent, however, it was found to have cardiotoxic side effects [28]. We reasoned that, given the dependence of TGFBR2 degradation on the BAG3-HSP70-CHIP axis, JG-98 may also exhibit pro-fibrotic effects. Wild-type iCFs were treated with JG-98 for 48 h and collagen 1, α-smooth muscle actin (αSMA), and vimentin expression were assessed by immunofluorescence. Each of these pro-fibrotic markers exhibited increased expression in JG-98 treated cells (Fig. 5A-D). The increased collagen expression upon inhibition of the BAG3-HSP70 axis was further investigated by assessing the total collagen secretion by picosirius red (Fig. 5E), Collagen I α1 secretion by ELISA (Supplementary Fig. 4 A), and *COL1A1* mRNA levels by

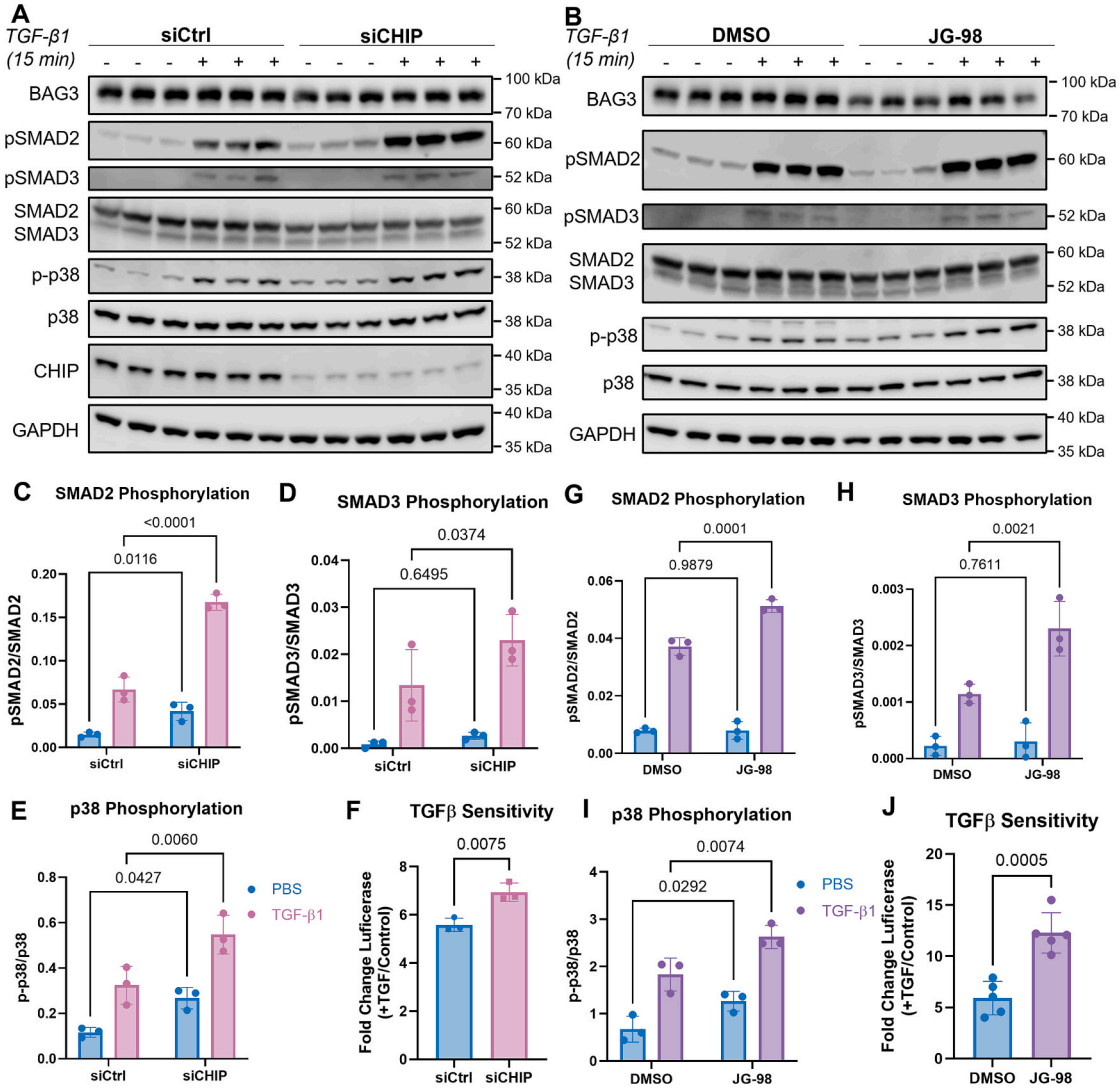


**Fig. 4.** Silencing of CHIP and disruption of the BAG3-HSP70 axis increases sensitivity to the TGF-β pathway. A) Western Blot of phosphorylation events downstream of TGFBR2 upon silencing of CHIP. B) Western Blot of phosphorylation events downstream of TGFBR2 upon pharmacological inhibition of the BAG3-HSP70 axis by JG-98. C-E) Densitometry quantification of phosphorylation of SMAD2 (C), SMAD3 (D), and p38 (E) upon silencing of CHIP from (A). F) SMAD-binding element 4 (SBE4) luciferase reporter shows increased sensitivity upon silencing of CHIP. G-I) Densitometry quantification of phosphorylation of SMAD2 (G), SMAD3 (H), and p38 (I) upon pharmacological inhibition of BAG3-HSP70 axis by JG-98 from (B). J) SMAD-binding element 4 (SBE4) luciferase reporter shows increased sensitivity with JG-98 induction. Significance indicated by student's *t*-test or two-way ANOVA with post-hoc Šídák. Error bars represent the mean with standard deviation. *p*-values less than 0.05 are considered statistically significant. For experiments A-I, $n = 3$, and for experiment J, $n = 5$, where n indicates a single well of cells, thus presenting biological replicates.

RT-qPCR (Fig. 5F), each showing increased expression upon addition of JG-98. Further investigation of pro-fibrotic transcriptional changes, as measured by RT-qPCR, revealed upregulation of fibronectin extra domain A (*FN-EDA*), the pro-fibrotic cytokine *IL-11* [29], and *ACTA2* (Fig. 5G-I). Moreover, mRNA of extracellular-matrix altering proteins *TIMP1*, *TIMP3*, and *LOX*, were significantly increased upon JG-98 exposure (Supplementary Fig. 4B-D). Interestingly, we observed an increase in the transcription of *CHIP* upon JG-98 exposure, suggesting a compensatory response (Supplementary Fig. 4E). Lastly, we observed a more proliferative phenotype of JG-98 treated cells by measuring Ki67 positively stained nuclei (Fig. 5J), which we previously found to be mediated by TGFBR2 [17]. Together, these results demonstrate that disruption of the BAG3-HSP70-CHIP activates a fibrogenic program in cardiac fibroblasts.

In summary, we have identified CHIP as an E3 ligase for TGFBR2 and established that the BAG3-HSP70 axis is required for its function in this context (Fig. 6).

## 4. Discussion

BAG3 was first identified in 2006 as a genetic locus associated with dilated cardiomyopathy (DCM) and with myocardial fibrosis [30]. Since then, germline loss-of-function mutations in BAG3 have been implicated in the development of cardiomyopathy [12]. Furthermore, loss of BAG3 has been observed in patients with non-genetic heart failure [16]. While cardiac fibrosis has traditionally been regarded as a consequence of cardiomyocyte cell death [31,32], we established a primary role of BAG3 in cardiac fibroblast homeostasis [17]. In the present study, we further elucidate the mechanistic underpinnings of this process.

We establish CHIP as an E3 ligase that BAG3 recruits to ubiquitinate TGFBR2 in cardiac fibroblasts through interaction with HSP70. These findings are in line with previous studies that show that CHIP regulates the TGF-β pathway. Specifically, CHIP has been identified as an E3 ligase of SMAD3 [9] and shown to modulate TGF-β signaling by facilitating ubiquitin-mediated degradation of SMAD3 [33]. HSP70 has been

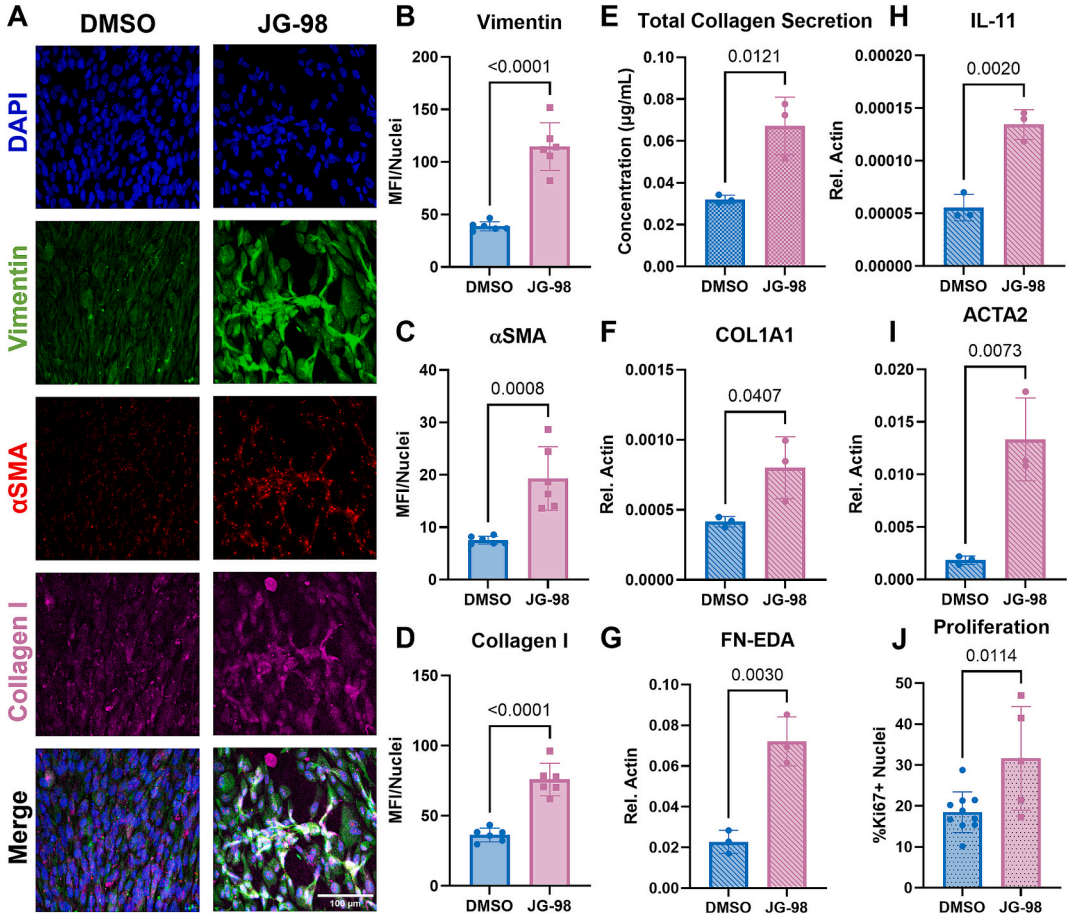


**Fig. 5.** Disruption of the BAG3-HSP70 axis by JG-98 increases fibrogenesis in cardiac fibroblasts. A) Immunofluorescent staining of Collagen I, α-smooth muscle actin, and vimentin treated with DMSO (control) and JG-98. B—D) Mean fluorescent intensity (MFI) of the Collagen I, α-smooth muscle actin, and vimentin stain normalized to the number of nuclei. E) Total collagen secretion as measured by a Picosirius red-based assay. F—I) RT-qPCR of COL1A1, FN-EDA, IL-11, and ACTA2 upon exposure to JG-98 in iCFs. H) Percentage of Ki67-positive nuclei upon exposure to JG-98. Significance indicated by unpaired two-tailed Student's *t*-test. Error bars represent the mean with standard deviation. *p*-values less than 0.05 are considered statistically significant. For immunofluorescence experiments (A-D), $n = 6$, where n indicates a single mounted slide (biological replicates) that was quantified 3 times (technical replicates), and the average is displayed in the graph. For experiment E, $n = 3$, where n indicates a single well of cells (biological triplicates). For experiments F—I, n = 3, where n indicates a single well of cells (biological triplicates), which was averaged from technical duplicates. For experiment J, $n = 5$ for JG-98 and $n = 10$ for DMSO, where n indicates a single cell of wells (biological replicates), which was imaged and averaged 3 times (technical replicates). (For interpretation of the references to colour in this figure legend, the reader is referred to the web version of this article.)

described in this pathway by facilitating the formation of the SMAD3-CHIP complex and thereby enhancing its ubiquitination and subsequent degradation [34].

While it has been previously established that BAG3 interacts with E3 ligases CHIP and WWP2, to facilitate protein degradation [18,25], three other E3 ubiquitin ligases, HECW1/2, RNF149, and RNF213, were also identified as direct interactors of BAG3 [17]. Experimentally, we confirmed that while CHIP and WWP2 both bind BAG3 and HSP70, only CHIP interacts with TGFBR2. This raises the interesting possibility that BAG3 and HSP70 recruit different E3 ligases depending on the specific client protein. RNF149 and RNF213 have both been shown to interact with the established pathways in differing cell types. RNF149 facilitates the degradation of CHIP in neurons [35] and RNF213 gene silencing upregulates TGF-β1 ligand levels through an unidentified mechanism in bone marrow-derived mesenchymal stem cells to induce Moyamoya disease [36]. Thus, while these E3 ligases have not been associated with BAG3 nor fibrosis, they pose avenues for further research.

This study was able to assess the unique role of BAG3 in cardiac fibroblasts by utilizing iPSC-derived CFs from a healthy wild-type donor and their isogenic BAG3 knock-out. We observed a contribution of each functional domain of BAG3 in TGFBR2 protein stability, suggesting that each domain is independently responsible for BAG3 function. Unsurprisingly, the most prominent role seems to be in the BAG domain, necessary for BAG3-HSP70 interaction [18,37], with clinical implications for patients with mutations in the BAG domain, such as the common E455K mutation [12,38]. The exact mechanism by which the other domains stabilize TGFBR2 remains unknown but may be related to hindered BAG3 activity.

Silencing CHIP increases the stability of TGFBR2 and TGF-β sensitivity, promoting the fibrogenic program in cardiac fibroblasts. Pharmacological inhibition of the BAG3-HSP70 axis by JG-98 has a similar effect, inducing IL-11 and ACTA2 expression and increasing collagen I secretion. These results are in line with previous *in vitro* work of the Kirk group on BAG3 in primary cardiac fibroblasts [39], in addition to our own work [17]. Other *in vitro* studies that examined components of the BAG3-HSP70-CHIP axis in cardiac fibroblasts did not investigate pro-fibrotic effects [40,41]. *In vivo,* we have shown the effects of BAG3-HSP70 loss in human myocardium from DCM patients with truncating variants of BAG3 that do not bind HSP70. Examining these tissues revealed increased levels of collagen deposition and fibrosis [17,31]. In addition, single-nuclei sequencing of these human hearts revealed a distinctive sensitivity to TGF-β signaling, accompanied by increased expression of IL-11 [17]. IL-11 has been previously established as a crucial pro-fibrotic agent [29], corroborating the pro-fibrotic effect of

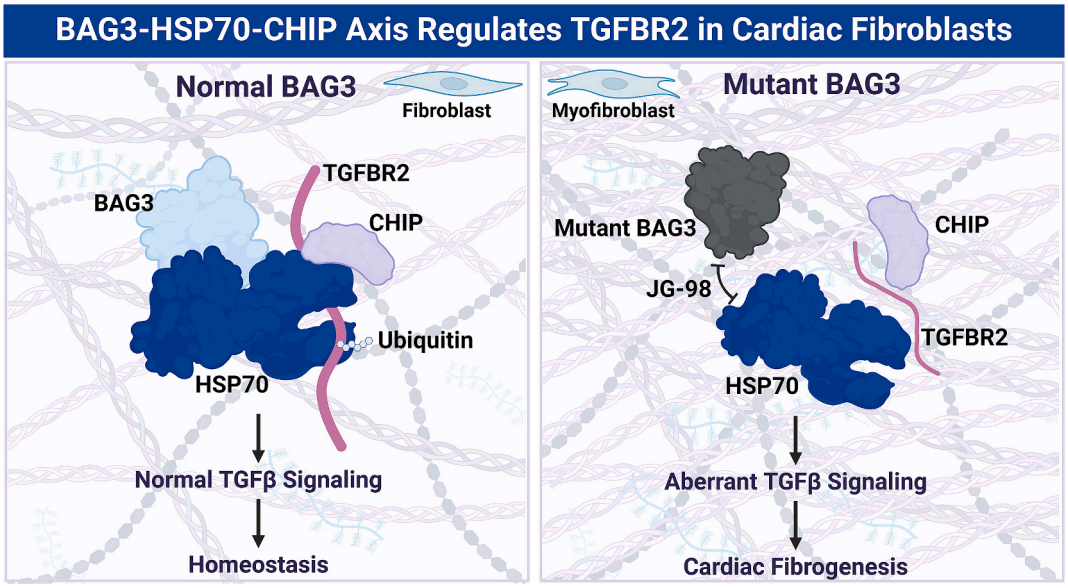


**Fig. 6.** Schematic representation of the proposed mechanism: BAG3-HSP70-CHIP axis regulates TGFBR2 in cardiac fibroblasts and maintains ECM homeostasis. However, mutations in BAG3 or pharmacological inhibition of the BAG3-HSP70 axis by JG-98 lead to aberrant TGF-β signaling, which can lead to cardiac fibrogenesis.

JG-98 through the induction of IL-11 transcription.

JG-98 was initially reported as a potential therapeutic for malignancies [42], however, a recent study has suggested potential cardiotoxicity due to BAG3's action in cardiomyocytes [28]. Here, we extend the evidence of its cardiotoxicity to cardiac fibroblasts, further suggesting off-target effects of JG-98. As such, therapeutic strategies relying on the inhibition of the BAG3-HSP70 axis, such as cancer treatments, should consider the pro-fibrotic effects of JG-98, especially since the composition and stiffness of the cancer-associated ECM play a large role in cancer progression and efficacy of cancer treatment [43,44].

Although monolayer studies limit the ability to assess structural changes in the collagen and ECM stiffness, we demonstrated upregulation of tissue inhibitor of metalloproteinase-1 (TIMP1), ACTA2, and lysyl oxidase (LOX). These genes are known to promote myocardial fibrosis through myofibroblast activation and collagen crosslinking [45–47]. This highlights the need for further investigation into the role of the BAG3-HSP70-CHIP axis in modulating the ECM beyond increased collagen secretion. Additionally, these pro-fibrotic gene expression changes enable the release of latent TGFβ [48], which, in conjunction with elevated levels of TGFBR2, may have a synergistic effect on fibrogenesis.

In summary, this study reveals the role of BAG3 and its complex formation with HSP70 and CHIP in the development and progression of cardiac fibrogenesis. Our findings raise the possibility of stabilizing f the BAG3-HSP70-CHIP axis as a therapeutic target for cardiac fibrosis. Previous studies have shown that HSP70 overexpression protects against pulmonary fibrosis in multiple mouse models [49,50]. Similar studies of CHIP overexpression have been performed in mice for hepatic fibrosis [51,52], while extracellular vesicles encapsulating CHIP have been shown to alleviate collagen deposition and renal fibrosis when delivered to the kidney [53]. The therapeutic potential of stabilization of the BAG3-HSP70-CHIP axis is further emphasized by the downregulation of BAG3 protein levels in patients with heart failure [16], thereby not limiting this therapeutic avenue to patients harboring pathogenic variants of BAG3.

The current study is limited by the use of relatively simple *in vitro* monolayers, derived from a single pair of male hiPSC, to investigate the BAG3-HSP70-CHIP axis. Given that fibrosis is a multifaceted disease involving multicellular signaling pathways and can take months to develop, future studies using more physiologically relevant models, such as engineered heart tissues or mice, are required to further elucidate the role of the BAG3-HSP70-CHIP axis in cardiac fibrosis.

## Resource availability

Original Western blots and raw data are provided in the supplement. The mass spectrometry proteomics data have been deposited to the ProteomXchange Consortium *via* the PRIDE partner repository with the dataset identifier PXD050740 from our previously published study [17]. Any additional information required to reanalyze the data reported in this paper is available from the lead contact upon request.

## AI disclosure

The authors declare that AI-assisted technology was not used in the preparation of this work.

## CRediT authorship contribution statement

**Margaretha A.J. Morsink:** Writing – review & editing, Writing – original draft, Methodology, Investigation, Formal analysis, Conceptualization. **Josephine M. Watkins:** Writing – review & editing, Investigation. **Katelyn Zhu:** Investigation. **Xiaokan Zhang:** Writing – review & editing, Methodology, Investigation. **Lori J. Luo:** Investigation. **Barry M. Fine:** Writing – review & editing. **Bryan Z. Wang:** Writing – review & editing, Investigation, Conceptualization. **Gordana Vunjak-Novakovic:** Writing – review & editing, Supervision, Resources, Project administration, Investigation, Funding acquisition.

## Declaration of Competing Interest

The authors declare no competing interests.

## Acknowledgments

We gratefully acknowledge the funding support of NIH (grants P41EB027062, UH3 EB025765 and R01HL076485 to GVN) and the American Heart Association (Predoctoral Fellowship 1018398 to MAJM; https://doi.org/10.58275/AHA.23PRE1018398.pc.gr.161141). We also

gratefully acknowledge the expert support of the core facilities for Confocal Microscopy and Proteomics at Columbia University. We thank Dr. Bruce Conklin (USCF, Gladstone Institute) for his generous sharing of reagents.

## Appendix A. Supplementary data

Supplementary data to this article can be found online at https://doi.org/10.1016/j.yjmcc.2025.06.003.

## References

[1] J.G. Travers, F.A. Kamal, J. Robbins, K.E. Yutzey, B.C. Blaxall, Cardiac Fibrosis, Circ. Res. 118 (2016) 1021–1040, https://doi.org/10.1161/CIRCRESAHA.115.306565.
[2] T.R. Eijgenraam, H.H.W. Silljé, R.A. de Boer, Current understanding of fibrosis in genetic cardiomyopathies, Trends Cardiovasc. Med. 30 (2020) 353–361, https://doi.org/10.1016/j.tcm.2019.09.003.
[3] X. Meng, D.J. Nikolic-Paterson, H.Y. Lan, TGF-β: the master regulator of fibrosis, Nat. Rev. Nephrol. 12 (2016) 325–338, https://doi.org/10.1038/nrneph.2016.48.
[4] J. Massagué, D. Sheppard, TGF-β signaling in health and disease, Cell 186 (2023) 4007–4037, https://doi.org/10.1016/j.cell.2023.07.036.
[5] L. Kubiczkova, L. Sedlarikova, R. Hajek, S. Sevcikova, TGF-β – an excellent servant but a bad master, J. Transl. Med. 10 (2012) 183, https://doi.org/10.1186/1479-5876-10-183.
[6] K.C. Flanders, Smad3 as a mediator of the fibrotic response, Int. J. Exp. Pathol. 85 (2004) 47–64, https://doi.org/10.1111/j.0959-9673.2004.00377.x.
[7] M. Scheffner, U. Nuber, J.M. Huibregtse, Protein ubiquitination involving an E1-E2-E3 enzyme ubiquitin thioester cascade, Nature 373 (1995) 81–83, https://doi.org/10.1038/373081a0.
[8] H. Chen, A. Moreno-Moral, F. Pesce, N. Devapragash, M. Mancini, E.L. Heng, M. Rotival, P.K. Srivastava, N. Harmston, K. Shkura, O.J.L. Rackham, W.-P. Yu, X.-M. Sun, N.G.Z. Tee, E.L.S. Tan, P.J.R. Barton, L.E. Felkin, E. Lara-Pezzi, G. Angelini, C. Beltrami, M. Pravenec, S. Schafer, L. Bottolo, N. Hubner, C. Emanueli, S.A. Cook, E. Petretto, WWP2 regulates pathological cardiac fibrosis by modulating SMAD2 signaling, Nat. Commun. 10 (2019) 3616, https://doi.org/10.1038/s41467-019-11551-9.
[9] L. Li, H. Xin, X. Xu, M. Huang, X. Zhang, Y. Chen, S. Zhang, X.-Y. Fu, Z. Chang, CHIP mediates degradation of Smad proteins and potentially regulates Smad-induced transcription, Mol. Cell. Biol. 24 (2004) 856–864, https://doi.org/10.1128/MCB.24.2.856-864.2004.
[10] L. Izzi, L. Attisano, Regulation of the TGFbeta signalling pathway by ubiquitin-mediated degradation, Oncogene 23 (2004) 2071–2078, https://doi.org/10.1038/sj.onc.1207412.
[11] E. Stürner, C. Behl, The role of the multifunctional BAG3 protein in cellular protein quality control and in disease, Front. Mol. Neurosci. 10 (2017), https://doi.org/10.3389/fnmol.2017.00177 null.
[12] F. Domínguez, S. Cuenca, Z. Bilińska, R. Toro, E. Villard, R. Barriales-Villa, J. Ochoa, F. Asselbergs, A. Sammani, M. Franaszczyk, M. Akhtar, M.J. Coronado-Albi, D. Rangel-Sousa, J. Rodríguez-Palomares, J. Jiménez-Jáimez, J.M. García-Pinilla, T. Ripoll-Vera, M.V. Mogollón-Jiménez, A. Fontalba-Romero, D. García-Medina, J. Palomino-Doza, D. de Gonzalo-Calvo, M. Cicerchia, J. Salazar-Mendiguchía, C. Salas, S. Pankuweit, T. Hey, J. Mogensen, P. Barton, P. Charron, P. Elliott, P. García-Pavía, Mutations., Dilated Cardiomyopathy Due to BLC2-Associated Athanogene 3 (BAG3), J. Am. Coll. Cardiol. 72 (20) (2018) 2471–2481, https://doi.org/10.1016/j.jacc.2018.08.2181.
[13] N. Norton, D. Li, M. Rieder, J. Siegfried, E. Rampersaud, S. Züchner, S. Mangos, J. Gonzalez-quintana, L. Wang, S. McGee, J. Reiser, E. Martin, D. Nickerson, R. Hershberger, Genome-wide studies of copy number variation and exome sequencing identify rare variants in BAG3 as a cause of dilated cardiomyopathy, Am. J. Hum. Genet. 88 (3) (2011) 273–282, https://doi.org/10.1016/j.ajhg.2011.01.016.
[14] A. Feldman, J. Gordon, J. Wang, J. Song, X. Zhang, V.D. Myers, D. Tomar, G. Gerhard, K. Khalili, J. Cheung, Novel BAG3 variants in African American patients with cardiomyopathy: reduced β-adrenergic responsiveness in excitation-contraction, J. Cardiac Failure null (2020), https://doi.org/10.1016/j.cardfail.2020.09.009 null.
[15] V.D. Myers, J. McClung, J. Wang, F.G. Tahrir, M. Gupta, J. Gordon, C.H. Kontos, K. Khalili, J. Cheung, A. Feldman, The multifunctional protein BAG3, JACC: basic to translational, Science 3 (2018) 122–131, https://doi.org/10.1016/j.jacbts.2017.09.009.
[16] T.G. Martin, V.D. Myers, P. Dubey, S. Dubey, E. Perez, C.S. Moravec, M.S. Willis, A. M. Feldman, J.A. Kirk, Cardiomyocyte contractile impairment in heart failure results from reduced BAG3-mediated sarcomeric protein turnover, Nat. Commun. 12 (2021) 2942, https://doi.org/10.1038/s41467-021-23272-z.
[17] B.Z. Wang, M.A.J. Morsink, S.W. Kim, L.J. Luo, X. Zhang, R.K. Soni, R.I. Lock, J. Rao, Y. Kim, A. Zhang, M. Neyazi, J.M. Gorham, Y. Kim, K. Brown, D. M. DeLaughter, Q. Zhang, B. McDonough, J.M. Watkins, K.M. Cunningham, G. Y. Oudit, B.M. Fine, C.E. Seidman, J.G. Seidman, G. Vunjak-Novakovic, Cardiac fibroblast BAG3 regulates TGFBR2 signaling and fibrosis in dilated cardiomyopathy, J. Clin. Invest. 135 (2025), https://doi.org/10.1172/JCI181630.
[18] V. Arndt, N. Dick, R. Tawo, M. Dreiseidler, D. Wenzel, M. Hesse, D.O. Fürst, P. Saftig, R. Saint, B.K. Fleischmann, M. Hoch, J. Höhfeld, Chaperone-assisted selective autophagy is essential for muscle maintenance, Curr. Biol. 20 (2010) 143–148, https://doi.org/10.1016/j.cub.2009.11.022.
[19] A.B. Meriin, A. Narayanan, L. Meng, I. Alexandrov, X. Varelas, I.I. Cissé, M. Y. Sherman, Hsp70–Bag3 complex is a hub for proteotoxicity-induced signaling that controls protein aggregation, Proc. Natl. Acad. Sci. 115 (2018) E7043–E7052, https://doi.org/10.1073/pnas.1803130115.
[20] L.M. Judge, J.A. Pérez-Bermejo, A. Truong, A. Ribeiro, J.C. Yoo, C.L. Jensen, M. Mandegar, N. Huebsch, R.M. Kaake, P. So, D. Srivastava, B. Pruitt, N. Krogan, B. Conklin, A BAG3 chaperone complex maintains cardiomyocyte function during proteotoxic stress, JCI Insight 2 (14) (2017), https://doi.org/10.1172/jci.insight.94623 null.
[21] H. Zhang, L. Tian, M. Shen, C. Tu, H. Wu, M. Gu, D.T. Paik, J.C. Wu, Generation of quiescent cardiac fibroblasts from human induced pluripotent stem cells for in vitro Modeling of cardiac fibrosis, Circ. Res. 125 (2019) 552–566, https://doi.org/10.1161/CIRCRESAHA.119.315491.
[22] P.W. Burridge, A. Holmström, J.C. Wu, Chemically defined culture and cardiomyocyte differentiation of human pluripotent stem cells, Curr. Protoc. Hum. Genet. 87 (2015) 21.3.1–21.3.15, https://doi.org/10.1002/0471142905.hg2103s87.
[23] X. Zhang, B.Z. Wang, M. Kim, T.R. Nash, B. Liu, J. Rao, R. Lock, M. Tamargo, R. K. Soni, J. Belov, E. Li, G. Vunjak-Novakovic, B. Fine, STK25 inhibits PKA signaling by phosphorylating PRKAR1A, Cell Rep. 40 (2022) 111203, https://doi.org/10.1016/j.celrep.2022.111203.
[24] C. McQuin, A. Goodman, V. Chernyshev, L. Kamentsky, B.A. Cimini, K.W. Karhohs, M. Doan, L. Ding, S.M. Rafelski, D. Thirstrup, W. Wiegraebe, S. Singh, T. Becker, J. C. Caicedo, A.E. Carpenter, CellProfiler 3.0: Next-generation image processing for biology, PLoS Biol. 16 (2018) e2005970, https://doi.org/10.1371/journal.pbio.2005970.
[25] N. Zhang, Y. Zhang, W. Miao, C. Shi, Z. Chen, B. Wu, Y. Zou, Q. Ma, S. You, S. Lu, X. Huang, J. Liu, J. Xu, L. Cao, Y. Sun, An unexpected role for BAG3 in regulating PARP1 ubiquitination in oxidative stress-related endothelial damage, Redox Biol. 50 (2022) 102238, https://doi.org/10.1016/j.redox.2022.102238.
[26] C. Klimek, B. Kathage, J. Wördehoff, J. Höhfeld, BAG3-mediated proteostasis at a glance, J. Cell Sci. 130 (2017) 2781–2788, https://doi.org/10.1242/jcs.203679.
[27] S. Murata, Y. Minami, M. Minami, T. Chiba, K. Tanaka, CHIP is a chaperone-dependent E3 ligase that ubiquitylates unfolded protein, EMBO Rep. 2 (2001) 1133–1138, https://doi.org/10.1093/embo-reports/kve246.
[28] T.G. Martin, C.E. Delligatti, N.A. Muntu, M.J. Stachowski-Doll, J.A. Kirk, Pharmacological inhibition of BAG3-HSP70 with the proposed cancer therapeutic JG-98 is toxic for cardiomyocytes, J. Cell. Biochem. 123 (2022) 128–141, https://doi.org/10.1002/jcb.30140.
[29] S. Schafer, S. Viswanathan, A.A. Widjaja, W.-W. Lim, A. Moreno-Moral, D. M. DeLaughter, B. Ng, G. Patone, K. Chow, E. Khin, J. Tan, S.P. Chothani, L. Ye, O. J.L. Rackham, N.S.J. Ko, N.E. Sahib, C.J. Pua, N.T.G. Zhen, C. Xie, M. Wang, H. Maatz, S. Lim, K. Saar, S. Blachut, E. Petretto, S. Schmidt, T. Putoczki, N. Guimarães-Camboa, H. Wakimoto, S. van Heesch, K. Sigmundsson, S.L. Lim, J. L. Soon, V.T.T. Chao, Y.L. Chua, T.E. Tan, S.M. Evans, Y.J. Loh, M.H. Jamal, K. K. Ong, K.C. Chua, B.-H. Ong, M.J. Chakaramakkil, J.G. Seidman, C.E. Seidman, N. Hubner, K.Y.K. Sin, S.A. Cook, IL-11 is a crucial determinant of cardiovascular fibrosis, Nature 552 (2017) 110–115, https://doi.org/10.1038/nature24676.
[30] P.T. Ellinor, S. Sasse-Klaassen, S. Probst, B. Gerull, J.T. Shin, A. Toeppel, A. Heuser, B. Michely, D.M. Yoerger, B.-S. Song, B. Pilz, G. Krings, B. Coplin, P.E. Lange, G. W. Dec, H.C. Hennies, L. Thierfelder, C.A. MacRae, A novel locus for dilated cardiomyopathy, diffuse myocardial fibrosis, and sudden death on chromosome 10q25-26, J. Am. Coll. Cardiol. 48 (2006) 106–111, https://doi.org/10.1016/j.jacc.2006.01.079.
[31] R. Toro, A. Pérez-Serra, Ó. Campuzano, J. Moncayo-Arlandi, C. Allegue, A. Iglesias, A. Mangas, R. Brugada, Familial dilated cardiomyopathy caused by a novel frameshift in the BAG3 gene, PLoS One 11 (2016), https://doi.org/10.1371/journal.pone.0158730 null.
[32] T.P. Thomas, L.A. Grisanti, The dynamic interplay between cardiac inflammation and fibrosis, Front. Physiol. 11 (2020) 529075, https://doi.org/10.3389/fphys.2020.529075.
[33] H. Xin, X. Xu, L. Li, H. Ning, Y. Rong, Y. Shang, Y. Wang, X.-Y. Fu, Z. Chang, CHIP controls the sensitivity of transforming growth factor-β Signaling by modulating the basal level of Smad3 through ubiquitin-mediated degradation*, J. Biol. Chem. 280 (2005) 20842–20850, https://doi.org/10.1074/jbc.M412275200.
[34] Y. Shang, X. Xu, X. Duan, J. Guo, Y. Wang, F. Ren, D. He, Z. Chang, Hsp70 and Hsp90 oppositely regulate TGF-β signaling through CHIP/Stub1, Biochem. Biophys. Res. Commun. 446 (2014) 387–392, https://doi.org/10.1016/j.bbrc.2014.02.124.
[35] J. Kim, M. de Haro, I. Al-Ramahi, L.L. Garaicoechea, H.-H. Jeong, J.Y. Sonn, B. Tadros, Z. Liu, J. Botas, H.Y. Zoghbi, Evolutionarily conserved regulators of tau identify targets for new therapies, Neuron 111 (2023) 824–838.e7, https://doi.org/10.1016/j.neuron.2022.12.012.
[36] C. Wang, C. Sun, Y. Zhao, H. Song, Z. Li, F. Jin, C. Cui, RNF213 gene silencing upregulates transforming growth factor β1 expression in bone marrow-derived mesenchymal stem cells and is involved in the onset of Moyamoya disease, Exp. Ther. Med. 22 (2021) 1024, https://doi.org/10.3892/etm.2021.10456.
[37] T.A. Colvin, V.L. Gabai, J. Gong, S.K. Calderwood, H. Li, S. Gummuluru, O. N. Matchuk, S.G. Smirnova, N.V. Orlova, I.A. Zamulaeva, M. Garcia-Marcos, X. Li, Z.T. Young, J.N. Rauch, J.E. Gestwicki, S. Takayama, M.Y. Sherman, Hsp70-Bag3 interactions regulate cancer-related signaling networks, Cancer Res. 74 (2014) 4731, https://doi.org/10.1158/0008-5472.CAN-14-0747.

[38] X. Fang, J. Bogomolovas, T. Wu, W. Zhang, C. Liu, J. Veevers, M. Stroud, Z. Zhang, X. Ma, Y. Mu, D. Lao, N. Dalton, Y. Gu, C. Wang, M. Wang, Y. Liang, S. Lange, K. Ouyang, K. Peterson, S. Evans, J. Chen, Loss-of-function mutations in co-chaperone BAG3 destabilize small HSPs and cause cardiomyopathy, J. Clin. Invest. 127 (2017) 3189–3200, https://doi.org/10.1172/JCI94310.

[39] T.G. Martin, L.A. Sherer, J.A. Kirk, BAG3 localizes to mitochondria in cardiac fibroblasts and regulates mitophagy, Am. J. Physiol. Heart Circ. Physiol. 326 (2024) H1124–H1130, https://doi.org/10.1152/ajpheart.00736.2023.

[40] S. Schuster, E. Heuten, A. Velic, J. Admard, M. Synofzik, S. Ossowski, B. Macek, S. Hauser, L. Schöls, CHIP mutations affect the heat shock response differently in human fibroblasts and iPSC-derived neurons, Dis. Model. Mech. 13 (2020) dmm045096, https://doi.org/10.1242/dmm.045096.

[41] J. Nylandsted, M. Rohde, K. Brand, L. Bastholm, F. Elling, M. Jäättelä, Selective depletion of heat shock protein 70 (Hsp70) activates a tumor-specific death program that is independent of caspases and bypasses Bcl-2, Proc. Natl. Acad. Sci. 97 (2000) 7871–7876, https://doi.org/10.1073/pnas.97.14.7871.

[42] X. Li, T. Colvin, J.N. Rauch, D. Acosta-Alvear, M. Kampmann, B. Dunyak, B. Hann, B.T. Aftab, M. Murnane, M. Cho, P. Walter, J.S. Weissman, M.Y. Sherman, J. E. Gestwicki, Validation of the Hsp70–Bag3 protein–protein interaction as a potential therapeutic target in cancer, Mol. Cancer Ther. 14 (2015) 642–648, https://doi.org/10.1158/1535-7163.MCT-14-0650.

[43] X. He, B. Lee, Y. Jiang, Extracellular matrix in cancer progression and therapy, Med. Rev. 2 (n.d.) (2021) 125–139, https://doi.org/10.1515/mr-2021-0028.

[44] E. Henke, R. Nandigama, S. Ergün, Extracellular matrix in the tumor microenvironment and its impact on Cancer therapy, Front. Mol. Biosci. 6 (2020), https://doi.org/10.3389/fmolb.2019.00160.

[45] C. Rodríguez, J. Martínez-González, The role of Lysyl oxidase enzymes in cardiac function and Remodeling, Cells 8 (2019) 1483, https://doi.org/10.3390/cells8121483.

[46] A. Takawale, P. Zhang, V.B. Patel, X. Wang, G. Oudit, Z. Kassiri, Tissue inhibitor of matrix Metalloproteinase-1 promotes myocardial fibrosis by mediating CD63–integrin β1 interaction, Hypertension 69 (2017) 1092–1103, https://doi.org/10.1161/HYPERTENSIONAHA.117.09045.

[47] Y. Li, C. Li, Q. Liu, L. Wang, A.X. Bao, J.P. Jung, S. Dodlapati, J. Sun, P. Gao, X. Zhang, J. Francis, J.D. Molkentin, X. Fu, Loss of *Acta2* in cardiac fibroblasts does not prevent the myofibroblast differentiation or affect the cardiac repair after myocardial infarction, J. Mol. Cell. Cardiol. 171 (2022) 117–132, https://doi.org/10.1016/j.yjmcc.2022.08.003.

[48] M. Shi, J. Zhu, R. Wang, X. Chen, L. Mi, T. Walz, T.A. Springer, Latent TGF-β structure and activation, Nature 474 (2011) 343–349, https://doi.org/10.1038/nature10152.

[49] S. Hagiwara, H. Iwasaka, S. Matsumoto, T. Noguchi, H. Yoshioka, Association between heat stress protein 70 induction and decreased pulmonary fibrosis in an animal model of acute lung injury, Lung 185 (2007) 287–293, https://doi.org/10.1007/s00408-007-9018-x.

[50] K.-I. Tanaka, Y. Tanaka, T. Namba, A. Azuma, T. Mizushima, Heat shock protein 70 protects against bleomycin-induced pulmonary fibrosis in mice, Biochem. Pharmacol. 80 (2010) 920–931, https://doi.org/10.1016/j.bcp.2010.05.025.

[51] J. Wang, H. Zhang, L. Chen, K. Fu, Y. Yan, Z. Liu, CircDCBLD2 alleviates liver fibrosis by regulating ferroptosis via facilitating STUB1-mediated PARK7 ubiquitination degradation, J. Gastroenterol. 59 (2024) 229–249, https://doi.org/10.1007/s00535-023-02068-6.

[52] Z. Mao, J. Zhao, F. Cui, Z. Li, J. Cao, J. Zhou, M. Hou, Z. Qian, STUB1 increases adiponectin expression by inducing ubiquitination and degradation of NR2F2, thereby reducing hepatic stellate cell activation and alleviating non-alcoholic fatty liver disease, Tissue Cell 88 (2024) 102345, https://doi.org/10.1016/j.tice.2024.102345.

[53] C. Ji, J. Zhang, L. Shi, H. Shi, W. Xu, J. Jin, H. Qian, Engineered extracellular vesicle-encapsulated CHIP as novel nanotherapeutics for treatment of renal fibrosis, Npj Regen. Med. 9 (2024) 1–11, https://doi.org/10.1038/s41536-024-00348-0.